THE JOURNAL OF PHYSICAL CHEMISTRY C

Article

pubs.acs.org/JPCC

Hydrocarbon Chain Length Induces Surface Structure Transitions in Alkanethiolate–Gold Adatom Self-Assembled Monolayers on Au(111)

P. Carro,*[,†] E. Pensa,[‡] C. Vericat,[‡] and R. C. Salvarezza[‡]

[†]Departamento de Química Física, Instituto de Materiales y Nanotecnología, Universidad de La Laguna, Avda. Astrofísico Francisco Sánchez S/N, La Laguna 38071, Tenerife, Spain

[‡]Instituto de Investigaciones Fisicoquímicas Teóricas y Aplicadas, Facultad de Ciencias Exactas, Universidad Nacional de La Plata, CONICET, Sucursal 4 Casilla de Correo 16, (1900) La Plata, Argentina

ABSTRACT: A detailed density functional calculation (DFT) study including van der Waals (vdW) dispersion forces of different adatom-containing models (RS–Au_{ad}–SR) at saturation coverage for methanethiol (MT), butanethiol (BT), and hexanethiol (HT) on Au(111) is presented. The stability analysis of these lattices shows a transition from the (3×4) to the $c(4 \times 2)$ surface structure when the number of C atoms in the alkanethiol chain is larger than 2, fairly predicting recent experimental observations for these systems. The transition takes place when the smaller energy needed to reconstruct the Au(111) surface and the larger binding energy for MT in the (3×4) MT lattice is compensated by a larger interaction energy between hydrocarbon chains in the $c(4 \times 2)$ lattice for BT and HT. Our calculations therefore explain why the (3×4) lattice is more stable for MT and ethanethiol (ET) while the $c(4 \times 2)$ lattice predominates for longer alkanethiols, thus shedding light on the behavior of alkanethiol self-assembled monolayers (SAMs) on Au(111).

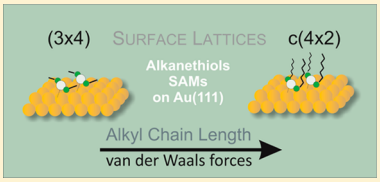

INTRODUCTION

Thiol self-assembled monolayers (SAMs) on Au(111) have been established as a model system in modern surface science, in addition to their numerous applications in nanotechnology.[1] These molecules adsorb on the gold surface as thiolates, yielding ordered commensurate lattices, the most usual being the $(\sqrt{3} \times \sqrt{3})$-R30° and its related $c(4 \times 2)$ superlattice, also known as the $(3 \times 2\sqrt{3})$ lattice, which can sometimes coexist on the same surface. Both lattices have thiolate surface coverage at saturation $\theta = 0.33$ and nearest-neighbor distances between molecules of ≈ 0.5 nm.[2]

The early picture of a simple organized monolayer on the unreconstructed Au(111) surface was challenged by some experimental results from synchrotron techniques.[3−5] Since then, and up to present, the so-called adatom models, which provide a new picture of the S–Au interface based on the formation of some kind of gold adatom (Au_{ad})–thiolate (RS) complex with a considerable reconstruction of the Au(111) surface, have aroused great interest and provoked a considerable controversy.[2]

Among the different models proposed,[2,5] the ones that are most widely accepted are those that involve RS–Au_{ad}–SR units based on scanning tunneling microscopy (STM) results at low coverage[6] and X-ray diffraction of thiolate-capped gold nanoclusters.[7] These models could provide an attractive unified view of the gold–thiolate interface, as they describe the $c(4 \times 2)$ lattice on planar (111) surfaces and also the surface structure of gold nanoclusters.[7,8] Other models involving RS–Au_{ad} units have also been proposed to describe both the $(\sqrt{3} \times \sqrt{3})$-R30° and $c(4 \times 2)$ lattices.[2]

Methanethiol (MT) adsorption on Au(111) has concentrated most of the experimental and theoretical efforts to elucidate this controversy because it is the simplest thiol. However, experimental data are contradictory, as $(\sqrt{3} \times \sqrt{3})$-R30°,[9,10] $c(4 \times 2)$,[11] and (3×4)[12,13] lattices have all been reported for adsorption on the Au(111) surface. In particular, recent STM data[12,13] for MT and ethanethiol (ET) give direct evidence of RS–Au_{ad}–SR moieties on the Au(111) surface at saturation coverage. More interesting, the (3×4) lattice with RS–Au_{ad}–SR species has been observed only for short thiols, because it is replaced by the $c(4 \times 2)$ and $(\sqrt{3} \times \sqrt{3})$-R30° lattices as the number of C atoms in the hydrocarbon chain is increased.

With regard to theoretical studies, the surface structure of MT on the Au(111) surface has been extensively studied in the frame of Au adatom models by using density functional theory (DFT).[2,14] Results have shown that surface models containing RS–Au_{ad}–SR moieties fairly explain the $c(4 \times 2)$ MT surface structure due to their higher thermodynamic stability in terms of the free energy. In contrast, little is known about the stability of the (3×4) lattice in the context of the other MT models. In fact, some DFT calculations show that the (3×4) lattice is more stable than a diluted $(3 \times 4\sqrt{3})$ by ≈ 0.12 eV per RS–Au_{ad}–SR moiety, a figure that is consistent with their coexistence on the Au surface as observed by STM.[13] On the other hand, recent molecular dynamics calculations for MT have suggested that, due to fast adatom diffusion, a scenario

Received: November 1, 2012
Revised: December 28, 2012
Published: January 3, 2013

dx.doi.org/10.1021/jp310800e | J. Phys. Chem. C 2013, 117, 2160−2165

where each c(4 × 2) cell contains solid-phase Au_{ad} at room temperature is unlikely.[15] To our knowledge, a comparative stability analysis based on DFT calculations between the dense (3 × 4) and c(4 × 2) lattices consisting of RS−Au_{ad}−SR species has not been performed until now. The situation is more complicated in the case of the ($\sqrt{3} \times \sqrt{3}$)R30° lattice consisting of RS−Au_{ad} moieties, as this becomes more unstable than the same MT lattice on unreconstructed Au(111) (without Au_{ad}).[2]

The theoretical study of longer alkanethiols on Au(111) introduces new challenges: van der Waals (vdW) dispersion forces need to be considered because they could have a strong influence on the organization and stability of the adsorbates in the SAM. In fact, it has been reported that vdW interactions stabilize the surface structures,[16] although these DFT calculations have been limited to a ($\sqrt{3} \times \sqrt{3}$)-R30° lattice and also for a nonreconstructed Au(111) surface (without Au adatoms). On the other hand, DFT molecular dynamic calculations for the c(4 × 2) MT and hexanethiol (HT) lattices containing a mixture of RS−Au_{ad}−SR, adsorbed RS species, and vacancies including vdW interactions has been performed, also revealing the role of the hydrocarbon chains in stabilize the lattices.[17] Moreover, an important improvement in the calculations is a recent work that models the effect of vdW dispersive forces in a c(4 × 2) superstructure consisting of RS−Au_{ad}−SR complexes as a function of the hydrocarbon chain length.[18] Results from that paper reveal the greater stability of the SAMs as the hydrocarbon chain is increased and the role of attractive interactions between RS−Au_{ad}−SR complexes at shorter distances.

Therefore, under this scenario new questions can be added to the existing controversy of the complex thiolate−Au(111) interface: Is it possible that MT organizes into different surface structures with similar stability, thus justifying the different experimental results? Why is the (3 × 4) structure observed only for short thiols such as MT and ET? Are vdW forces playing a role in selecting the surface structures as the hydrocarbon chain is increased? And what is the chemistry of the surface species: RS−Au_{ad}−SR or RS−Au_{ad}?

Because the thiol surface coverage and the number of thiolate−Au bonds are the same for all surfaces structures ($\theta = {}^1/_3$), a detailed theoretical study of the stability for different adatom-containing thiolate lattices opens the possibility to explain and predict surface structure transitions in thiolate−Au_{ad}-containing lattices as a function of the number of C atoms in the hydrocarbon chain.

In this work we have made vdW-DFT calculations to investigate the role of hydrocarbon chain length for selecting the surface structure (that contains thiolate−Au_{ad} species) for MT, BT, and HT on the Au(111) surface. We present the first evidence that vdW forces are responsible for the surface structure transition experimentally observed in RS−Au_{ad}−SR-containing lattices. Moreover, our stability analysis opens the possibility for the coexistence of different reconstructions on the same surface, thus explaining the different experimental results reported for the MT SAMs. In addition, we have studied the ($\sqrt{3} \times \sqrt{3}$)-R30° lattice with RS−Au_{ad} moieties for comparison, giving the possibility to test the effect of a different surface chemistry (RS−Au_{ad}−SR vs RS−Au_{ad}) in the stability of alkanethiol SAMs. Note that although this comparison has already been made for MT,[6,8] it has not been yet performed for longer alkanethiols, where vdW interactions could have a critical role. Once again, we have found that RS−Au_{ad}−SR species in (3 × 4) and c(4 × 2) lattices are highly favored over RS−Au_{ad} in the ($\sqrt{3} \times \sqrt{3}$)-R30° lattice.

METHODS AND EXPERIMENTAL DETAILS

Density Functional Theory Calculations. Density functional theory calculations have been performed with the periodic plane-wave basis set code VASP 5.2.[19,20] We have followed the scheme of nonlocal functionals proposed by Dion et al.,[21] vdW-DFT, and the optimized Becke88 exchange functional optB88-vdW[22] to take into account van der Waals interactions. This functional has been successfully used to study others adsorption processes.[23,24] We have also compared these results to others that do not include vdW interactions by using the Perdew−Burke−Ernzerhof (PBE) functional of generalized gradient approximation (GGA). The electronic wave functions were expanded in a plane-wave basis set with 420 eV cutoff energy. The projector-augmented plane wave (PAW) method has been used to represent the atomic cores with PBE potential.

Gold surfaces were represented by a five-atomic-layer slab with 12 Å vacuum. Optimal grids of k-points of 5 × 4 × 1 have been used for both (3 × 4) and (3 × $2\sqrt{3}$) supercells. Alkanethiol radical species were optimized in an asymmetric box of 10 Å × 12 Å × 14 Å. Because of the large unit cell size, Brillouin zone integration was carried out at the Γ point only. The calculated lattice constants are 4.16 Å (optB88-vdW) and 4.17 Å (PBE), in good agreement with the experimental value (4.078 Å).[25] The binding energy E_b is calculated as

$$E_b = \frac{1}{N_{thiol}}[E^{thiol/Au} - E^{R}_{Au(111)} - N_{thiol}E_{thiol}] \quad (1)$$

where $E^{thiol/Au}$, $E^{R}_{Au(111)}$, and E_{thiol} stand for total energy of the adsorbate−substrate system, total energy of Au slab when RS moieties are removed, and the alkanethiol radical, respectively, whereas N_{thiol} is the number of thiolate radicals in the surface unit cell. In all cases $N_{thiol} = 4$ [also for the RS−Au_{ad} model for the ($\sqrt{3} \times \sqrt{3}$)R30° BT lattice]. Because Au adatoms in both surface models are in bridge position (Figure 2) but this site is not a stable minimum, $E^{R}_{Au(111)}$ has been calculated by allowing only a constrained relaxation of the Au adatoms.[18] A negative number indicates that adsorption is exothermic with respect to the separate clean surface and thiol radical.

Materials. Hexanethiol (Fluka, 97%) and absolute ethanol (Carlo Erba, 99.5%) were used as received. Evaporated Au films on glass with (111) preferred orientation (AF 45 Berliner Glass KG, Germany) were used as substrates. After annealing for 3 min with a hydrogen flame, these Au substrates exhibit atomically smooth (111) terraces separated by steps of monatomic height, as revealed by scanning tunneling microscopy (STM).

Hexanethiol Self-Assembled Monolayer Preparation. HT SAMs were formed on the Au(111) substrates by immersion of the clean substrates in deaerated 50 μM HT ethanolic solutions for 24 h. Then the samples were removed from the solution, rinsed with the solvent, dried with N_2, and imaged in air by STM.

Scanning Tunneling Microscopy. In-air STM experiments were performed in the constant current mode with an ECM scanning probe microscope from Veeco Instruments (Bruker, Santa Barbara, CA) controlled by a Nanoscope IIIA unit, also from Veeco Instruments. Mechanically cut Pt−Ir tips were used and typical bias voltages (E_{bias}), set-point currents, and scan rates were 0.5−0.8 V, 0.5−0.8 nA, and 1−30 Hz,

dx.doi.org/10.1021/jp310800e | J. Phys. Chem. C 2013, 117, 2160−2165

respectively. The scanner calibration was checked by imaging highly oriented pyrolytic graphite (HOPG) with atomic resolution.

RESULTS AND DISCUSSION

First, we briefly discuss the motivation for the use of RS−Au_{ad}−SR moieties for alkanethiols SAMs with C atom number between 1 and 6. Indeed, while the presence of thiolate−Au_{ad} species on MT and ET SAMs at saturation coverage forming (3 × 4) lattices has been recently well documented,[9,11−13] the presence of RS−Au_{ad}−SR moieties in longer alkanethiol SAMs such as HT needs careful justification. In fact, although some evidence supporting the presence of these species have been given from analysis of the gold adatom island coverage after hydrogen desorption of longer alkanethiol SAMs,[26,27] the progressive increment of the $(\sqrt{3} \times \sqrt{3})$-R30° domains with increasing length of the hydrocarbon chain turns the interpretation of the data more complex. Therefore, we decided to analyze the surface coverage of vacancy islands (θ_{vac}) on HT-covered large terraces to estimate the amount of Au_{ad} needed to form the thiolate−Au_{ad} species on the Au(111) surface. In particular we have used top-rounded large terraces (Figure 1)

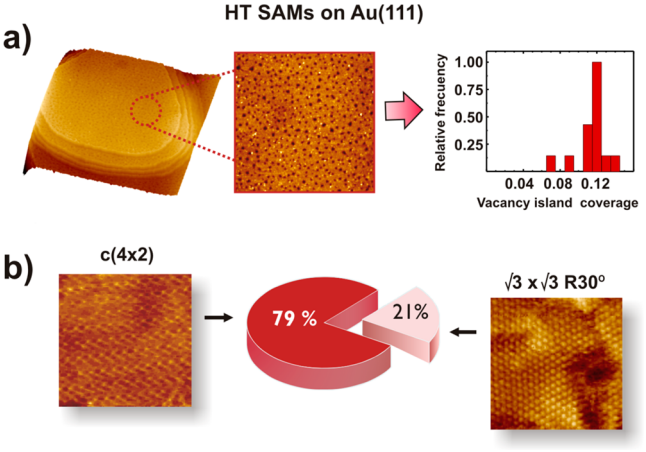

Figure 1. Hexanethiol SAMs on Au(111). (a, left) Three-dimensional image (331 × 331 nm^2) showing rounded, concentric gold terraces separated by monatomic steps. (a, center) Image (150 × 150 nm^2) corresponding to a zoom of the top-rounded terrace. Vacancy islands are observed as dark spots. (a, right) Histogram of vacancy island coverage, built with information from STM images of large HT-covered top-rounded Au terraces corresponding to 24 different samples. (b, center) Pie chart showing HT lattice proportion. (b, left and right) High-resolution STM images (10 × 10 nm^2) of (left) c(4 × 2) and (right) $(\sqrt{3} \times \sqrt{3})$-R30° lattices.

to calculate θ_{vac} because in this kind of terrace there is no chance of Au_{ad} contribution from step edges to form thiolate−Au_{ad} species, which would complicate estimation of the total amount of Au_{ad} arising from vacancy islands, as already discussed.[28] Note also that Au_{ad} produced by thiol adsorption should be confined to those terraces due to the Ehrlich−Schwoebel energy barrier at descending step edges,[29] which inhibits interlayer adatom diffusion. Therefore, in our measurements θ_{vac} can be validly used to estimate the total amount of Au_{ad} removed from the Au surface, and to estimate the stoichiometry of the thiolate−Au_{ad} complexes without significant contributions from step edges.

Results from our analysis show that although the average size of the vacancy islands can vary from sample to sample (data not shown), their coverage θ_{vac} is ≈ 0.12 (Figure 1). Therefore, we have surface Au_{ad} coverage θ_{ad} ≈ 0.12 arising from terraces and also an additional θ_{ad} ≈ 0.04 provided by the lifting of the herringbone Au(111) reconstruction.[13] This results in θ_{ad} ≈ 0.16, a figure that is in excellent agreement with the theoretically expected value for the staple model (RS−Au_{ad}−SR) and far from that expected for the RS−Au_{ad} model. In fact, for alkanethiolate coverage $\theta = {}^1/_3$, θ_{ad} is ≈ 0.16 if RS−Au_{ad}−SR species are present and θ_{ad} = 0.33 for RS−Au_{ad} moieties. It should be noted that the c(4 × 2) surface structure, which is consistent with the RS−Au_{ad}−SR species, largely predominates over the $(\sqrt{3} \times \sqrt{3})$-R30° structure (Figure 1), supporting the presence of these species as the main component in HT SAMs. It should also be noted that our experimental data for Au_{ad} are in excellent agreement with those reported from gas-phase alkanethiol desorption.[26,27] Also, BT, an intermediate case, yields mainly the c(4 × 2) lattice,[30] thus justifying the description of these lattices in terms of RS−Au_{ad}−SR moieties.[31] In contrast to the case of longer alkanethiols, the c(4 × 2) lattice is spontaneously formed for BT and HT and predominates over other possible lattices, and thus no annealing is needed.[28]

In the next step we present our DFT calculations for the (3 × 4) and c(4 × 2) lattices consisting of RS−Au_{ad}−SR motifs. Figure 2 shows the optimized structures with optB88-vdW functional for (a, b) MT, (c, d) BT, and (e, f) HT in the (3 × 4) (left panel) and c(4 × 2) (right panel) configurations. In all cases we have found that the Au adatoms of the RS−Au_{ad}−SR moieties lie on bridge sites of the Au surface, while the S atoms are bound not only to the Au adatom but also to the Au surface at nearly on-top positions.

Detailed structural information from the vdW-DFT calculations performed is displayed in Table 1, where we analyze the S−Au_{ad}−S angle, α(S−Au_{ad}−S); the tilt of the molecular axis (C−C direction on the same side of the chain) with respect to the surface normal, α_{tilt}; the angle between S−C_1 bond and the surface normal, α_1; the Au_{ad}−surface Au atom distance, d(Au_{ad}−Au_{surf}); the S−Au adatom distance, d(S−Au_{ad}); and the S−surface Au atom distance, d(S−Au_{surf}). In order to compare the relevant results, all these geometrical parameters have been averaged between equivalent positions. We have found no significant differences in either d(S−Au_{surf}) or α(S−Au_{ad}-S) for MT, BT, and HT in both (3 × 4) and c(4 × 2) surface structures. However, the α_{tilt} values change not only with the chain length but also with the surface structure. In fact, this angle is ≈ 67° for MT in the c(4 × 2) and (3 × 4) lattices, ≈ 13−15° for BT and HT in the (3 × 4) lattice, and 32−34° for BT and HT in c(4 × 2). While BT and HT in the c(4 × 2) lattice show α_{tilt} values close to those experimentally found in alkanethiol SAMs (≈ 30°),[32] BT and HT in the (3 × 4) lattice exhibit much smaller and unrealistic α_{tilt} values (≈ 13−15°). The variation of α_{tilt} when the chain length is increased in the c(4 × 2) lattice is in good agreement with results reported from DFT calculations for unreconstructed $(\sqrt{3} \times \sqrt{3})$R30°.[16] Indeed, it is well-known[16] that the tilt angle leads to important variations in the molecular conformation at the surface. In fact, for the c(4 × 2) lattice, the α_1 value in MT (Table 1) indicates that the S−C_1 bond is slightly closer to the Au surface than for BT and HT, whose α_1 values are similar. In contrast, for the (3 × 4) structure, the α_1 value in HT reveals that the S−C_1 bond

dx.doi.org/10.1021/jp310800e | J. Phys. Chem. C 2013, 117, 2160−2165

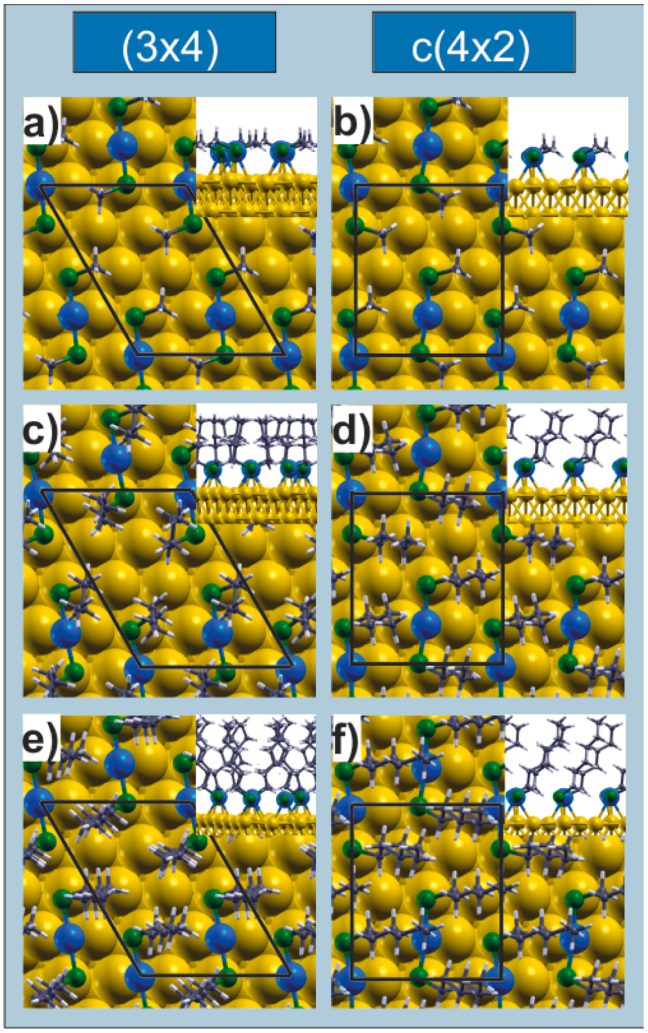

Figure 2. Optimized surface structures (optB88-vdW). Left panel: (3 × 4) configurations of (a) MT, (c) BT, and (e) HT. Right panel: c(4 × 2) surface structure of (b) MT, (d) BT, and (f) HT. (Insets) Lateral views of each of the different surface structures. Green, S; black, C; white, H; blue, Au adatom; yellow, Au. The corresponding unit cells are drawn in each panel (solid black lines).

is farther from the surface than those corresponding to MT and BT due to steric constraints.

The E_b values of MT, BT, and HT in the different lattices have also been included in Table 1. As expected, vdW interactions play a relevant role in the adsorption process: E_b values markedly increase (become more negative) with increasing alkyl chain length. Our calculations show that the adsorption of MT is slightly stronger in the (3 × 4) lattice than in the c(4 × 2) surface structure, as the binding energy difference ΔE_b $[E_b(\mathrm{vdW})_{c(4\times2)} - E_b(\mathrm{vdW})_{(3\times4)}]$ is only +0.01 eV. This is not surprising because these surface structures are, in principle, rather similar in terms of all structural parameters (Table 1).

In contrast, for BT and HT, the binding energy difference between both lattices is reverted and increases with hydrocarbon chain length (ΔE_b is −0.08 eV for BT and −0.14 eV for HT). This behavior can be rationalized in terms of the increasing difficulty to organize longer hydrocarbon chains in the (3 × 4) structure due to steric hindrance.[33]

There are also some other interesting conclusions. First, in going from the c(4 × 2) and (3 × 4) BT structures to the corresponding HT structures, vdW forces add ≈ 0.105 eV/CH_2 unit for the c(4 × 2) lattice and ≈ 0.075 eV/CH_2 unit for the (3 × 4) lattice; these figures are on the order of those experimentally measured for chain−chain interactions in alkanethiol SAMs (≈0.08−0.04 eV/CH_2 unit).[1,34,35] The smaller estimated values in the experiments can be explained by considering that real SAMs show chain disorder and a large amount of surface defects.[36] On the other hand, the lower value found in the vdW-DFT calculations for the (3 × 4) lattice when compared with c(4 × 2) is consistent with the fact that hydrocarbon chain interactions cannot adopt the best configuration.[33]

However, as already discussed,[6,37] the binding energy is not a valid criterion to predict the stability of the different surface structures, since it does not consider the energy cost to reconstruct the Au(111) surface; that is, the energy required to remove the Au adatoms needed to form the RS−Au_{ad}−SR moieties. Therefore, in order to estimate the stability of the different arrangements for HT, BT, and MT on the Au(111) surface, we have compared two energetic terms: on one hand, the cost to form the reconstructed surface per unit cell, E_{rec}, and on the other hand, the gain of stability when N_{thiol} thiols bind to the surface unit cell, $N_{thiol}E_b$. The reconstruction energy per unit cell for the different surfaces has been calculated as

$$E_{rec} = E^{R}_{Au(111)} - E^{U}_{Au(111)} - n_{ad}E^{Au}_{bulk} \quad (2)$$

Table 1. Energetic (optB88-vdW and PBE) and Structural Data (optB88-vdW) of Methanethiol, Butanethiol, and Hexanethiol SAMs on Au(111)

	MT		BT		HT	
	c(4 × 2)	(3 × 4)	c(4 × 2)	(3 × 4)	c(4 × 2)	(3 × 4)
E_b (optB88-vdW),[a] eV	−2.91	−2.92	−3.28	−3.20	−3.49	−3.35
E_b (PBE),[b] eV	−2.38	−2.40	−2.34	−2.31	−2.33	−2.18
d (Au_{ad}−Au_{surf}),[c] Å	2.95	2.96	2.94	2.94	2.94	2.93
d (S−Au_{surf}),[d] Å	2.52	2.53	2.54	2.53	2.54	2.52
d (S−Au_{ad}),[e] Å	2.34	2.34	2.34	2.34	2.34	2.34
α (S−Au_{ad}−S),[f] deg	169.0	175.6	168.6	174.0	168.6	175.7
α_{tilt},[g] deg	68.0	67.3	34.4	12.7	32.2	15.3
α_1,[h] deg	68.0	67.3	62.5	64.8	63.5	54.6

[a]Binding energy obtained *with* dispersion forces among alkyl chains in alkanethiol SAMs. [b]Binding energy obtained *without* dispersion forces among alkyl chains in alkanethiol SAMs. [c]Au_{ad}−surface Au atom distance. [d]S−surface Au atom distance. [e]S−surface Au adatom distance. [f]S−Au_{ad}−S angle. [g]Tilt of the molecular axis with respect to the surface normal. [h]Angle between S−C_1 bond and the surface normal.

dx.doi.org/10.1021/jp310800e | J. Phys. Chem. C 2013, 117, 2160−2165

Table 2. Comparative Stability of Different Surface Structures

	MT		BT			HT	
	c(4 × 2)	(3 × 4)	c(4 × 2)	(3 × 4)	($\sqrt{3} \times \sqrt{3}$)R30°	c(4 × 2)	(3 × 4)
$N_{thiol}E_b$, eV	−11.64	−11.68	−13.12	−12.84	−10.60	−13.96	−13.40
E_{rec}, eV	+2.08	+2.04	+2.08	+2.04	+2.98	+2.08	+2.04
$N_{thiol}E_b + E_{rec}$, eV	−9.56	−9.64	−11.04	−10.80	−7.62	−11.88	−11.36

where $E^{U}_{Au(111)}$ corresponds to the energy of the unreconstructed Au(111) surface, calculated in the same unit cell as that used for the $E^{R}_{Au(111)}$ estimation, and E^{Au}_{bulk} is the total energy of a bulk Au atom, while n_{ad} is the number of Au adatoms in the surface unit cell. Thus, E_{rec} is the energy related to Au adatom formation, which yields the RS−Au−SR moieties, and in order to account for the stability of the different surface structures for MT, BT, and HT, $N_{thiol}E_b + E_{rec}$ (Table 2) is the value that should be considered.

Results in Table 2 show that the E_{rec} value needed to reconstruct the (3 × 4) lattice is 0.04 eV smaller than that needed to reconstruct the c(4 × 2) lattice. The same difference in E_{rec} has been estimated for RS−Au_{ad}−SR complexes in trans and cis configurations in the c(4 × 2) lattice by Ferrighi et al.[18] employing a meta-GGA functional. For MT, an additional 0.04 eV/unit cell arises from the difference in E_b, favoring the (3 × 4) lattice (Table 1). Both contributions explain why the c(4 × 2) MT lattice is less stable than the (3 × 4) lattice by ≈ +0.08 eV/unit cell, thus supporting the experimental observations reported in ref 12.

Also, DFT calculations with the PBE functional, for which the effect of the hydrocarbon chains is negligible, show that E_b is favored for the (3 × 4) MT lattice.

It is interesting to note the key role of the substrate in determining the MT lattice, as DFT calculations for the RS−Au_{ad}−SR complexes in vacuum (in the absence of the Au substrate) give the opposite result: the *cis* configuration becomes more stable than the *trans* configuration by ≈ 0.13 eV. Therefore, the difference in stability of the adsorbed complexes at the Au surface should be carefully analyzed. While the *cis* and *trans* complexes in vacuum have a similar optimized value (≈176°) for α(S−Au_{ad}−S), this angle is slightly distorted when the *cis*-RS−Au_{ad}−SR complex [c(4 × 2) lattice] is adsorbed on Au surface, decreasing about 10° (Table 1). In contrast, the α(S−Au_{ad}−S) value for the *trans*-RS−Au_{ad}−SR complex adsorbed on the Au substrate [(3 × 4) lattice] remains unchanged with respect to the optimized value found in vacuum. In order to test the effect that this subtle difference implies in terms of stability, we have calculated the DFT energy for the RS−Au_{ad}−SR complexes frozen in the optimized geometries that they adopt on the Au surface, using an asymmetric box of 10 Å × 12 Å × 14 Å. In agreement with previous data,[38] our results show that that the adsorbed *trans* configuration [α(S−Au_{ad}−S) ≈ 176°] is more stable than the *cis* configuration [α(S−Au_{ad}−S) ≈ 169°], thus confirming that the geometric distortion induced by the substrate on the adsorbed cis complexes could be responsible for the slight decrease in stability of the c(4 × 2) lattice.

Now we will focus on the evolution of SAM stability as the hydrocarbon chain is increased. In contrast to MT, the c(4 × 2) lattice (*cis* configuration) is more stable than the (3 × 4) lattice (*trans* configuration) for BT and HT, as $N_{thiol}E_b + E_{rec}$ are more negative by −0.24 and −0.52 eV, respectively. In this case the greater cost to reconstruct the c(4 × 2) lattice is compensated by a larger binding to the surface and by the vdW forces resulting from a better optimization of hydrocarbon chain interactions. This last feature becomes more evident as the stability of the c(4 × 2) lattices markedly increases with the hydrocarbon chain length, as shown in Figure 3.

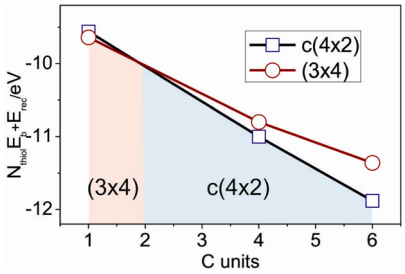

Figure 3. Stability diagram $N_{thiol}E_b + E_{rec}$ in electronvolts as a function of the hydrocarbon chain length (in C units). Note that the two lines intersect at C ≈ 2.

This diagram fairly predicts that the (3 × 4) lattice is slightly more stable for MT and ET, while the c(4 × 2) lattice predominates for longer alkanethiols (2 < C units ≤ 6). Moreover, the slight difference in stability between the (3 × 4) and c(4 × 2) lattices in short thiols opens the possibility of coexistence of different reconstructions on the same surface, thus explaining the experimental observations in MT SAMs.[11,12]

There is another interesting point to explain the effect of hydrocarbon chain length on stability of the different lattices. In Table 1 we have included DFT results without considering vdW interactions made by using the PBE functional. In this case E_b should reflect only the Au−S bond strength. These results show that while E_b remains almost constant for MT, BT, and HT in the c(4 × 2) structure, E_b decreases for the (3 × 4) lattice as the hydrocarbon chain is increased; that is, the Au−S bond strength becomes weaker. This distinct behavior in the absence of van der Waals interactions correlates with the behavior of the angle between the C_1−S bond and the surface normal, which shows the same trend in the presence of dispersive forces (see Table 1). Then, the large deviation of HT in the (3 × 4) lattice toward a small stability in Figure 3 can also be understood through steric hindrance to accommodate the hydrocarbon chains that also reflects in a weaker Au−S bond.

Finally, it is interesting to note that Woodruff and coworkers[9] have studied MT adsorption on Au(111) by X-ray standing waves. In that paper, the authors concluded that their experimental data could be explained by a model consisting of RS−Au_{ad} moieties in the ($\sqrt{3} \times \sqrt{3}$)-R30° configuration. While previous calculations have shown that this model is thermodynamically less favorable than a ($\sqrt{3} \times \sqrt{3}$)-R30° MT on an unreconstructed Au(111) surface,[2,37] it has been recently suggested that this model could be valid for intermediate and long alkanethiols,[12,39] where this lattice is frequently observed (Figure 1). We have calculated the BT−Au_{ad} adsorption on

dx.doi.org/10.1021/jp310800e | J. Phys. Chem. C 2013, 117, 2160−2165

Au(111) including vdW interaction forces. For a better comparison we have employed the c(4 × 2) unit cell with four BT−Au_{ad} moieties. Again, our DFT results show that the RS−Au_{ad} lattice is energetically unfavorable with respect to the corresponding RS−Au_{ad}−RS lattice by ≈3.4 eV (Table 2).

CONCLUSIONS

Our results can explain why MT and ET organize in (3 × 4) surface structures while intermediate thiols (2 < C units ≤ 6) organize in c(4 × 2) lattices. The (3 × 4) ⇒ c(4 × 2) lattice transition for alkanethiols with C units > 2 is driven by vdW dispersion forces among hydrocarbon chains, which are more important in the case of the c(4 × 2) surface structure, a fact that also reflects in a stronger Au−S bond. For both short and intermediate chain length alkanethiol SAMs, the formation of RS−Au_{ad}−SR species is highly favored. The slightly higher stability of the (3 × 4) over the c(4 × 2) MT lattices arises from both the smaller energy cost to reconstruct the Au(111) surface and the larger binding energy. This small difference in stability also explains why both lattices have been found by experimental observations on the Au(111) surface. The next challenge will be to include alkanethiols with longer hydrocarbon chains (C units ≥ 8) in the surface structure diagram, as they predominantly show the $(\sqrt{3} \times \sqrt{3})$-R30° lattice, a structure that present models cannot describe in terms of RS−Au_{ad}−SR complexes.[2]

AUTHOR INFORMATION

Corresponding Author

*E-mail pcarro@ull.es; phone +34 922 318031; fax +34 922 318002.

Notes

The authors declare no competing financial interest.

ACKNOWLEDGMENTS

We acknowledge financial support from ANPCyT (PICT 2554) and CONICET (PIP 00362), both from Argentina, and CTQ2011-24784 MICINN, Spain. E.P. acknowledges a doctoral fellowship from CONICET. P.C. thankfully acknowledges the computer resources provided by Atlante, Canary Islands Supercomputing Infrastructure, Red Española de Supercomputación.

REFERENCES

(1) Love, J. C.; Estroff, L. A.; Kriebel, J. K.; Nuzzo, R. G.; Whitesides, G. M. *Chem. Rev.* **2005**, *105*, 1103−1170.
(2) Pensa, E.; Cortés, E.; Corthey, G.; Carro, P.; Vericat, C.; Fonticelli, M. H.; Benítez, G.; Rubert, A. A.; Salvarezza, R. C. *Acc. Chem. Res.* **2012**, *45*, 1183−1192.
(3) Kondoh, H.; Iwasaki, M.; Shimada, T.; Amemiya, K.; Yokoyama, T.; Ohta, T.; Shimomura, M.; Kono, S. *Phys. Rev. Lett.* **2003**, *90*, No. 066102.
(4) Roper, M. G.; Skegg, M. P.; Fisher, C. J.; Lee, J. J.; Dhanak, V. R.; Woodruff, D. P.; Jones, R. G. *Chem. Phys. Lett.* **2004**, *389*, 87−91.
(5) Fenter, P.; Eberhardt, A.; Eisenberger, P. *Science* **1994**, *266*, 1216−1218.
(6) Maksymovych, P.; Sorescu, D. C.; Yates, J. T., Jr. *Phys. Rev. Lett.* **2006**, *97*, No. 146103.
(7) Jadzinsky, P. D.; Calero, G.; Ackerson, C. J.; Bushnell, D. A.; Kornberg, R. D. *Science* **2007**, *318*, 430−433.
(8) Grönbeck, H.; Häkkinen, H.; Whetten, R. L. *J. Phys. Chem. C* **2008**, *112*, 15940−15942.
(9) Yu, M.; Bovet, N.; Satterley, C. J.; Bengió, S.; Lovelock, K. R. J.; Milligan, P. K.; Jones, R. G.; Woodruff, D. P.; Dhanak, V. *Phys. Rev. Lett.* **2006**, *97*, No. 166102.
(10) Kondoh, H.; Nozoye, H. *J. Phys. Chem. B* **1999**, *103*, 2585−2588.
(11) Danışman, M. F.; Casalis, L.; Bracco, G.; Scoles, G. *J. Phys. Chem. B* **2002**, *106*, 11771−11777.
(12) Tang, L.; Li, F.; Zhou, W.; Guo, Q. *Surf. Sci.* **2012**, *606*, L31−L35.
(13) Voznyy, O.; Dubowski, J. J.; Yates, J. T.; Maksymovych, P. *J. Am. Chem. Soc.* **2009**, *131*, 12989−12993.
(14) Hakkinen, H. *Nat. Chem.* **2012**, *4*, 443−455.
(15) Longo, G. S.; Bhattacharya, S. K.; Scandolo, S. *J. Phys. Chem. C* **2012**, *116*, 14883−14891.
(16) Torres, E.; Blumenau, A. T.; Biedermann, P. U. *ChemPhysChem* **2011**, *12*, 999−1009.
(17) Cossaro, A.; Mazzarello, R.; Rousseau, R.; Casalis, L.; Verdini, A.; Kohlmeyer, A.; Floreano, L.; Scandolo, S.; Morgante, A.; Klein, M. L.; Scoles, G. *Science* **2008**, *321*, 943−946.
(18) Ferrighi, L.; Pan, Y.-x.; Grönbeck, H.; Hammer, B. *J. Phys. Chem. C* **2012**, *116*, 7374−7379.
(19) Kresse, G.; Hafner, J. *Phys. Rev. B* **1993**, *47*, 558−561.
(20) Kresse, G.; Furthmüller, J. *Comput. Mater. Sci.* **1996**, *6*, 15−50.
(21) Dion, M.; Rydberg, H.; Schröder, E.; Langreth, D. C.; Lundqvist, B. I. *Phys. Rev. Lett.* **2004**, *92*, No. 246401.
(22) Klimes, J.; Bowler, D. R.; Michaelides, A. *J. Phys. Condens Matter* **2010**, *22*, 022201.
(23) Lew, W.; Crowe, M. C.; Campbell, C. T.; Carrasco, J.; Michaelides, A. *J. Phys. Chem. C* **2011**, *115*, 23008−23012.
(24) Floridia Addato, M. A.; Rubert, A. A.; Benítez, G. A.; Fonticelli, M. H.; Carrasco, J.; Carro, P.; Salvarezza, R. C. *J. Phys. Chem. C* **2011**, *115*, 17788−17798.
(25) Pearson, W. B., *Handbook of Lattice Spacing and Structure of Metals*; Pergamon Press, Inc.: New York, 1958.
(26) Kautz, N. A.; Kandel, S. A. *J. Am. Chem. Soc.* **2008**, *130*, 6908−6909.
(27) Kautz, N. A.; Kandel, S. A. *J. Phys. Chem. C* **2009**, *113*, 19286−19291.
(28) Maksymovych, P.; Voznyy, O.; Dougherty, D. B.; Sorescu, D. C.; Yates, J. T., Jr. *Prog. Surf. Sci.* **2010**, *85*, 206−240.
(29) Schwoebel, R. L.; Shipsey, E. J. *J. Appl. Phys.* **1966**, *37*, 3682−3686.
(30) Terán Arce, F.; Vela, M. E.; Salvarezza, R. C.; Arvia, A. J. *Langmuir* **1998**, *14*, 7203−7212.
(31) Wang, Y.; Chi, Q.; Hush, N. S.; Reimers, J. R.; Zhang, J.; Ulstrup, J. *J. Phys. Chem. C* **2011**, *115*, 10630−10639.
(32) Schreiber, F. *Prog. Surf. Sci.* **2000**, *65*, 151−257.
(33) Voznyy, O.; Dubowski, J. J. *Langmuir* **2009**, *25*, 7353−7358.
(34) Dubois, L. H.; Zegarski, B. R.; Nuzzo, R. G. *J. Chem. Phys.* **1993**, *98*, 678−688.
(35) Dubois, L. H.; Nuzzo, R. G. *Annu. Rev. Phys. Chem.* **1992**, *43*, 437−463.
(36) Vericat, C.; Vela, M. E.; Salvarezza, R. C. *Phys. Chem. Chem. Phys.* **2005**, *7*, 3258−3268.
(37) Vericat, C.; Vela, M. E.; Benitez, G.; Carro, P.; Salvarezza, R. C. *Chem. Soc. Rev.* **2010**, *39*, 1805−1834.
(38) Dance, I. G. *Polyhedron* **1986**, *5*, 1037−1104.
(39) Li, F.-S.; Zhou, W.; Guo, Q. *Phys. Rev. B* **2009**, *79*, No. 113412.

NOTE ADDED AFTER ASAP PUBLICATION

This paper was published on the Web on January 15, 2013, with an error to reference 22 and the Methods and Experimental Details Section. The corrected version was reposted on January 24, 2013.